Case Studies in Thermal Engineering 60 (2024) 104568

Contents lists available at ScienceDirect

Case Studies in Thermal Engineering

journal homepage: www.elsevier.com/locate/csite

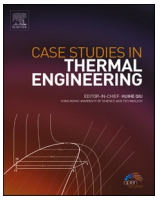

ANN and CFD driven research on main performance characteristics of solar chimney power plants: Impact of chimney and collector angle

Pinar Mert Cuce [a,b,c], Erdem Cuce [d,e,f,*], Dipak Kumar Mandal [g], Dilip Kumar Gayen [h], Muhammad Asif [i], Abdallah Bouabidi [j], Saad Alshahrani [k,l], Chander Prakash [m], Manzoore Elahi M. Soudagar [n]

[a] Department of Architecture, Faculty of Engineering and Architecture, Recep Tayyip Erdogan University, Zihni Derin Campus, 53100, Rize, Turkey
[b] Department of Energy Systems Engineering, Faculty of Engineering and Architecture, Recep Tayyip Erdogan University, Zihni Derin Campus, 53100, Rize, Turkey
[c] College of Built Environment, Birmingham City University, B4 7XG, Birmingham, UK
[d] Department of Mechanical Engineering, Faculty of Engineering and Architecture, Recep Tayyip Erdogan University, Zihni Derin Campus, 53100, Rize, Turkey
[e] School of Engineering and the Built Environment, Department of Mechanical Engineering, Birmingham City University, B4 7XG, Birmingham, UK
[f] Center for Research Impact & Outcome, Chitkara University, Rajpura, 140401, Punjab, India
[g] Department of Mechanical Engineering, Government Engineering College, Samastipur, Bihar, 848127, India
[h] Department of Computer Science Engineering, College of Engineering and Management, Kolaghat, 721171, India
[i] Department of Architectural Engineering and Construction Management, King Fahd University of Petroleum and Minerals, 31261, Dhahran, Saudi Arabia
[j] Mechanical, Modeling, Energy and Materials Research Unit, M2EM, National Engineering School of Gabes ENIG, University of Gabes Institution, Gabes, Tunisia
[k] Department of Mechanical Engineering, College of Engineering, King Khalid University, P.O. Box 394, Abha, 61421, Saudi Arabia
[l] Centre for Engineering and Technology Innovations, King Khalid University, Abha, 61421, Saudi Arabia
[m] University Centre for Research and Development, Chandigarh University, Mohali, Punjab, 140413, India
[n] Centre of Molecular Medicine and Diagnostics (COMManD), Saveetha Dental College and Hospitals Saveetha Institute of Medical and Technical Sciences, Saveetha University, Chennai, 600 077, India

* Corresponding author. Department of Mechanical Engineering, Faculty of Engineering and Architecture, Recep Tayyip Erdogan University, Zihni Derin Campus, 53100, Rize, Turkey.
E-mail addresses: pinar.mertcuce@erdogan.edu.tr (P.M. Cuce), erdem.cuce@erdogan.edu.tr (E. Cuce), dipkuma@yahoo.com (D.K. Mandal), dilipgayen@cemk.ac.in (D.K. Gayen), asifm@kfupm.edu.sa (M. Asif), bouabidi_abdallah@yahoo.fr (A. Bouabidi).

https://doi.org/10.1016/j.csite.2024.104568
Received 24 March 2024; Received in revised form 7 May 2024; Accepted 17 May 2024
Available online 22 May 2024
2214-157X/© 2024 The Authors. Published by Elsevier Ltd. This is an open access article under the CC BY license (http://creativecommons.org/licenses/by/4.0/).

GRAPHICAL ABSTRACT

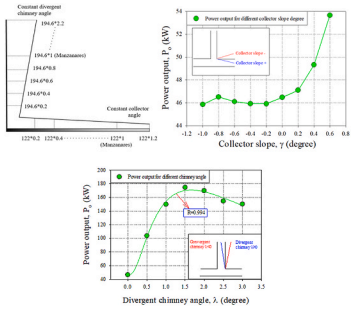

ARTICLE INFO

Handling Editor: Huihe Qiu

Keywords:
Solar chimney power plant
Divergent chimney
Collector angle
Optimum power
Design
ANN model

ABSTRACT

Solar energy systems operate directly connected to the sun. Solar chimney power plants are privileged systems that can provide power output even in cloudy weather and during hours when there is no sun. The design and sizing of this system, which researchers focused on after its first application in the 1980s, is very effective on its performance. In this study, the collector slope and chimney slope that give maximum power output for the Manzanares pilot plant are investigated with a 3D CFD model. Simulations made using the RNG k-e turbulence model and the DO (discrete ordinates) solar ray tracing algorithm provide results that are in high compatibility with experimental data and literature. It is understood that the system provides maximum power at 0.6° collector slope and 1.5° chimney divergence angle. It is seen that the system, which gives a power output of approximately 46 kW in the reference case, exceeds the power output by 4.5 times and reaches 216.853 kW in the design that includes the collector and chimney slope. The effects of the main elements of the system on the performance are also included by changing the collector radius and chimney height while preserving these inclination angles. More than the power output in the reference case, 49.233 kW, can be achieved with the inclined design, with a collector radius of 73.2 m and a chimney height of 155.68 m. Although the effect of increasing the chimney height on power output continues after 1.2 floors, its effect decreases. In the study, it is seen that increasing the chimney height and changing the collector radius provide a greater increase in power output. Furthermore, the scope extends to the incorporation of an Artificial Neural Network (ANN) model, presenting a novel approach to predicting SCPP system performance. The findings ascertain the utilisation of 9 neurons in the hidden layer of the ANN, demonstrating a precise alignment with the study data.

1. Introduction

The habit of collective living and urbanization brought about by globalization has caused the human population to concentrate in certain regions. This situation increases the importance of critical elements such as food, energy and cleaning day by day. In particular, the increase in energy needs day by day with the advancements of technology reveals the energy problem all over the world. Obtaining energy needs mostly from primary energy sources (fossil fuels) due to economic growth poses a great threat in terms of greenhouse gas emissions and global warming [1]. On the other hand, there are serious plans to control this situation and move towards renewable energy sources in the next 50–80 years through international cooperation and agreements [2]. In previous similar studies, serious targets were set regarding the rate of renewable energy use [3]. Although it has not yet reached the desired level, the use of renewable energy resources is being encouraged more and more every day and research on the subject is accelerating. So much so that in 2017, a quarter of the energy production in the world was obtained from renewable energy sources [4]. Renewable energy sources do not have high CO_2 emissions during use, like fossil fuels, and are environmentally friendly sources [5]. Although renewable energy sources are diverse, the main ones are solar energy, wind energy, bioenergy, geothermal energy, and hydropower [6]. Renewable energy sources are mostly used to generate electricity, but solar differs in the diversity of its usage areas. While the sun provides the opportunity to produce electricity directly or indirectly [7], its energy can also be used thermally for different purposes. By utilizing the thermal energy of the sun, solar cookers, solar dryers, solar pond, solar air condition, solar stills etc. systems can be used for different purposes [8]. On the other hand, it is possible to obtain electricity with solar chimney power plants (SCPP) by using the thermal energy of the sun [9]. These systems, also known as solar updraft tower (SUT), are designed to generate electricity by thermally utilizing solar energy [10]. The SCPP system consists of a collector, chimney, and turbine and operates according to basic physical laws. The sun is

transferred to the system through a semi-permeable collector. The collector both allows the sun to enter the system and retains the system air. Solar radiation transferred to the system air causes the temperature of the system air to increase. In addition, solar radiation reaches the ground and is thermally stored there. There is also an increase in temperature on the ground. The temperature increase on the floor creates convection heat transfer due to the temperature difference between the system air and the ground. The temperature of the system air, which is exposed to both direct radiation from the sun and heat transfer from the ground, increases. The system air, whose temperature increases, begins to move upwards with buoyancy effects depending on the density difference. The chimney collector, which is the second basic element of the system, is positioned in the centre. Due to its height, the density of the air at the entrance and exit is different, which creates a continuous upward movement effect at the entrance of the chimney. This effect, called the vacuum effect, forces the system air, which is exposed to buoyancy effects under the collector, to accelerate upwards from the chimney entrance. With this effect, system air is constantly drawn upwards in the chimney. Meanwhile, the turbine generator system located at a certain height produces electricity from the movement of the system air. The schematic view of the system is given in Fig. 1.

The history of SCPP is old in theory, but its implementation took place in the 1980s [11]. A team led by Professor Schlaich implemented the first prototype in the Manzanares region of Spain [12]. The first prototype, Manzanares SCPP, with its 194.6 m high chimney, 244 m diameter and 1.85 m high collector, continues to produce electricity for 7 years [13]. Theoretical calculations were confirmed in the experimental measurements obtained from the system, and 50 kW power output was obtained from the system in the middle of the day on 2 September 1982 [14]. After the Manzanares prototype, numerous studies were carried out on the performance and development of the system. When the studies are examined, it is seen that the majority of them are theoretical studies based on thermodynamics and heat transfer, small-scale experimental studies, and computer-based studies. The small scale of experimental studies is one of the difficulties in measuring the performance of the system due to cost. In particular, the experimental setup must be constantly updated to test the effect of dimensional changes on system performance. This situation creates difficulty. In addition, testing in the same climatic conditions has different difficulties. For this reason, theoretical and computer-supported studies are in majority. Initial theoretical studies are based on the Manzanares prototype, and researchers predict the performance of systems to be installed in different sizes [15–17]. SCPP differs from other solar energy systems. 24-hour power output can be obtained with the energy storage unit applied to the ground of the system [18]. With natural storage materials applied on the ground, continuous power output can be obtained while reducing costs [19].

2. Parameters affecting SCPP performance

SCPP is a solar energy system, although it can provide power output even when there is no sun. Naturally, it is affected by the intensity of solar radiation. Parameters called climatic parameters, which can vary depending on the region where the system is installed, are independent of the system. Since solar radiation intensity will directly increase the amount of energy entering the system, it is expected to increase the performance of the system. Test results obtained at the Manzanares pilot facility show that the system shows maximum performance in the middle of the day when solar radiation intensity is high [14]. Researchers evaluate the effect of solar radiation intensity on system performance by building prototypes of different sizes. They confirm that solar radiation intensity increases the performance of the system [20,21]. A comparison of the theoretical and CFD studies of the researchers for the Manzanares pilot plant and the effect of solar radiation intensity on system performance is given in Table 1. The results in the studies confirm that solar radiation intensity increases the performance of the system. Differences in results may be due to environmental temperature and some design differences. Experimental data are added to the table by averaging the data obtained from the pilot facility at different solar radiation intensities. Like solar radiation intensity, environmental temperature is one of the climatic parameters that affects the performance of the system. The increase in environmental temperature reduces the performance of the system under the same conditions. Researchers suggest that the Manzanares pilot plant will produce lower power output with increasing ambient temperature under the same conditions [22–24].

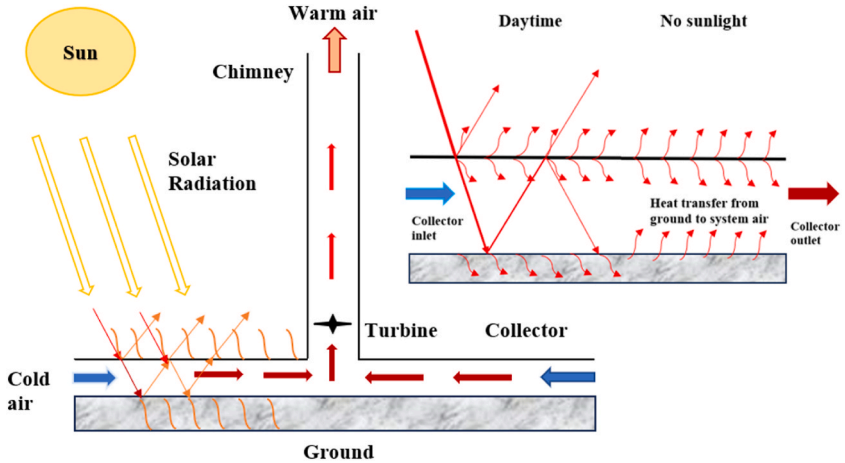

Fig. 1. Solar chimney power plant system (SCPP) or other name solar updraft tower (SUT) systems.

Climatic parameters depend on the location of the system and cannot be intervened later. Performance prediction can be made by analysing geometric and design parameters before the system is installed. Chimney height and collector diameter as geometric parameters are studied intensively by researchers. The chimney is the driving force of the system and increasing the height of the chimney provides a direct increase in performance. If the chimney height of the Manzanares pilot plant is made 500 m, the power output increases to 134 kW [28]. Some researchers claim that the performance of the system will constantly increase with the height of the chimney [29] while others claim that it is the maximum power output point [30,31]. Since the collector transfers solar radiation to the system, an increase in its size is expected to improve system performance. The pilot plant Manzanares consists of the collector with an area of 40,000 m^2 of glass and 6000 m^2 of plastic membrane [27]. It is widely accepted in the literature by researchers that increasing the collector size of the pilot plant will give more power output when other parameters are kept constant [8,32,33]. Karimipour-Fard, and Beheshti [34] claim that increasing the collector radius of the Manzanares pilot plant will increase the power output of the system exponentially, such that the power output of 42.5 kW in the reference case will exceed 4 times to 184.46 kW if the collector radius is made 300 m similarly, different researchers also express similar views [35]. There are also researchers who argue that there is a limitation for the collector size when other parameters are kept constant for the pilot plant, and that constantly increasing the collector radius will not increase the power output of the system after a point [30,36]. Apart from chimney height and collector radius, chimney diameter and collector height also affect system performance. In their studies based on the Manzanares pilot plant, researchers emphasize that there is a maximum size for the chimney diameter and after this point the power output will decrease [34,37]. Researchers emphasize that increasing the collector height will negatively affect the performance of the Manzanares pilot plant [34,37,38]. The effect of geometric parameters on the system are direct performance enhancing effects for collector radius and chimney height. The reason for this is that more pressure difference occurs with the increase in chimney height, and more energy enters the system as the collector radius increases. Increasing the diameter of the chimney allows more air to be discharged from the system, but there is a limitation in this situation. Increasing the collector height allows more air to be included in the system, but negatively affects the temperature increase under the collector. In addition to all these effects, effects arising from system design are also decisive in system performance. Collector slope or profile is an important parameter because it affects the movement of system air. Linear, parabolic, and cascade of the collector have significant impact on power output [39]. With a small-scale experimental prototype, researchers argue that when the collector outlet is kept at a constant height and the height of the collector inlet is increased, the air flow rate at the chimney entrance decreases [40,41]. The Manzanares pilot plant collector is horizontal in the reference case [15]. Studies based on the pilot plant claim that collector tilt improves the performance of the system but will have a negative effect after a point [42,43]. Like collector design, chimney design is also important for the system. It is seen in the literature that the chimney design is defined as the divergent and convergent chimney angle and the ratio of the chimney exit area to the chimney entrance area (AR) [8]. Increasing the chimney outlet diameter while keeping the chimney inlet diameter constant is called divergent chimney design and causes more air to be discharged from the system. In this case, the performance of the system is expected to increase. On the contrary, keeping the chimney inlet diameter constant and reducing the chimney exit area is called convergent chimney design and air discharge from the system is expected to decrease. In both cases, the chimney rises linearly. SCPP performance is evaluated not only with linear but also with parabolic chimney designs [44]. Researchers evaluate the effects of different chimney designs on SCPP performance through small-scale prototypes, theoretical, and CFD studies [45–47]. For the Manzanares pilot plant, researchers make evaluations based on convergent divergent chimney angle and AR, and their details are given in Table 2. Values are presented based on the maximum power output point for the pilot plant.

As can be seen from the table, there are different evaluations in the literature on divergent chimney design for the Manzanares pilot plant. These differences may be due to differences in climatic parameters. In the literature, the common point reached by researchers for both pilot plants and SCPPs of different sizes is that the chimney divergence angle for maximum system performance is in the range of 1–2° [49,52,53]. The AR value of this range is 2.8–5.5 for the Manzanares pilot plant.

In their groundbreaking study, Behara et al. [54]. conduct pioneering modelling and analysis to determine the optimal sizing of SCPP in real-world scenarios, considering the dispersed and irregular nature of solar energy. Unlike previous research, they examine various factors including storage thickness, air temperature variations, chimney inlet velocities, and mass flow rates. Their results indicate that increasing storage thickness leads to changes in these parameters. Additionally, they propose an approach for selecting the optimal combination from the sizing curve options, aiming to minimise costs.

In another investigation, Behara et al. [55] explore the impact of collector radius, chimney height, and storage thickness on optimal generator power. Their study identifies the optimal combination of these variables to be 100 m for collector radius, 300 m for chimney height, and 0.2 m for storage thickness, resulting in a power output of 7 kW. Furthermore, they record the maximum daily energy production at 112 kWh.

Table 1
Performance of the Manzanares pilot plant depending on solar radiation intensity.

Solar radiation (W/m^2)/Reference	Cuce et al., [22]	Guo et al., [25]	Hoseini and Mehdipour [26]	Experimental data [27]
200	7.7 kW	3.87 kW	–	9.6 kW
400	17.24 kW	14.9 kW	21.22 kW	17.8 kW
600	27.3 kW	26.32 kW	32.54 kW	26.2 kW
800	34.9 kW	37.55 kW	43.86 kW	34.4 kW
1000	49.06 kW	48.36 kW	56.6 kW	47.3 kW

Table 2
Details of divergent chimney design studies for the Manzanares pilot plant.

Standard power output, P_o (kW)	Divergent chimney degree, λ (°)	Area ratio (AR)	Power output with divergent chimney, P_o (kW)	Ref.
54.3	1.5	4.1	168.5	[48]
51.59	0.75	2.25	75.91	[49]
39.5	2.91	8.7	231.7	[50]
50.37	3.2	10	680	[51]
33.7	1	1.668	70.1	[52]

3. Purpose and objective of the study

There are many studies in the literature that analyse performance for the Manzanares pilot plant. Researchers reach similar results for the effects of climatic parameters on system. A similar situation applies to collector and chimney sizing. Geometric dimensioning has been interpreted many times by different researchers through experimental, theoretical, and CFD studies. Although there are a certain number of studies in the literature for chimney and collector design, the results are controversial. In this study, firstly, the ideal angle values for the collector and chimney slope are found for the Manzanares pilot plant. After the ideal angle values are found, the system performance is analysed in different configurations by changing the chimney height and collector size. An attempt is made to guide future studies by comparing the results with the literature. The schematic view of the work carried out is given in Fig. 2. Using the dimensions established for the Manzanares pilot plant, we have demonstrated that multiplying the value by a factor less than 1 leads to have convergent angle, whilst multiplication by a factor greater than 1 brings about having divergent chimney angle. In this investigation, we favoured the divergent angle chimney value based on performance data from existing literature. Additionally, Table 3 illustrates the parametric data regarding the alterations in power output resulting from adjustments made to the collector radius, divergent angle, and chimney height, as investigated in the study.

4. Mathematical model and CFD details

This study aims to interpret the optimum design parameters for maximum performance of the Manzanares pilot plant. Moving away from the traditional approach, an attempt is made to evaluate the collector size and chimney height with different designs. First, the optimum chimney divergence angle for the pilot plant is obtained. Then, considering the collector slope, the outputs of the system are evaluated with the divergent chimney inclined collector combination. By keeping the divergent chimney angle and collector slope constant, performance analysis is performed for different values of chimney height and collector radius. First, a 3D CFD model is created with the ANSYS FLUENT engineering commercial software student version. The 90° model is preferred for faster and more economical analysis. The model contains two symmetry planes, XZ and YZ. The created model, mesh image, and critical details are given in Fig. 3. Geometric dimensions belong to the Manzanares pilot facility, and since there is no temperature change after 1 m below the ground, the ground thickness is taken as 1 m [14].

The governing equations are solved simultaneously via FLUENT. The equations of continuity, momentum, and energy can be given as follows [56]:

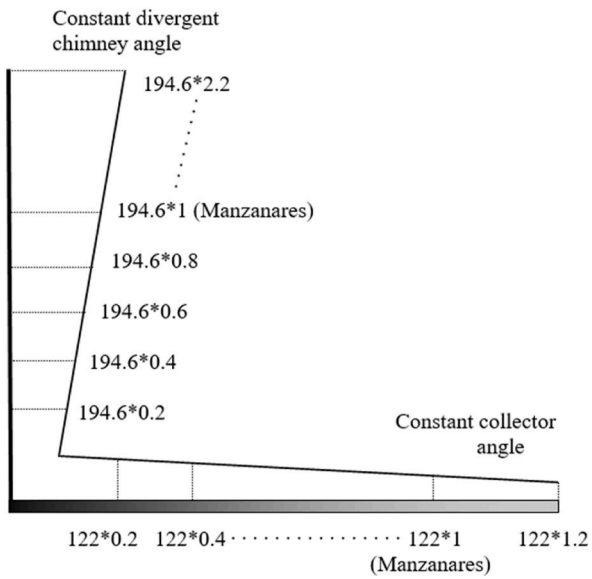

Fig. 2. SCPP schematic view of the working detail.

Table 3
Data parameters investigated in the study.

Dependency	Collector inlet, h_i	R_c	γ	h_c	λ	P_o (kW)
Variations in P_o corresponding to alterations in collector diameter	1.85	24.4	0	194.6	0	2.689676
		48.8				8.645723
		73.2				18.69576
		97.6				30.9754
		122				46.47228
		146				62.60344
		171				80.96169
		195				100.8881
Changes in P_o corresponding to variations in divergence angle	1.85	122	0	194.6	0.5	103.5238
					1	149.7841
					1.5	174.6959
					2	169.8436
					2.5	154.4866
					3	150.1495
Alterations in P_o corresponding to changes in chimney height	1.85	122	0	116.76	0	27.58896
				155.68		38.22506
				194.6		46.47228
				233.53		56.23583
				272.44		68.57303
				311.36		72.8178
				350.28		82.78565
				389.2		93.19116
				428.12		97.97282

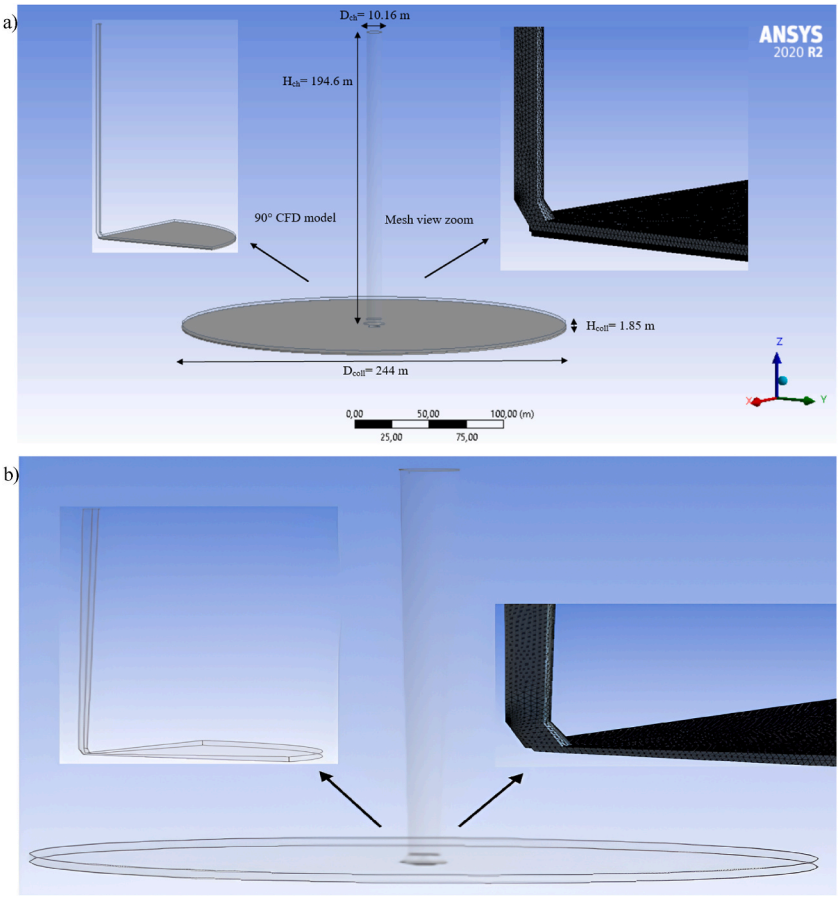

Fig. 3. a) 3D CFD view, geometrical dimensions, 90° CFD model, and mesh view, **b)** 3D view of 1.5° divergent chimney angle.

$$(\vec{\nabla}.\vec{v}) = 0 \tag{1}$$

$$\vec{v}\vec{\nabla}.\vec{v} = -\frac{1}{\rho_o}\vec{\nabla}P + \frac{\mu}{\rho_o}\vec{\nabla}^2\vec{v} + \vec{g}[1-\beta(T-T_o)] \tag{2}$$

$$\vec{v}\vec{\nabla}T = a_f\vec{\nabla}^2T \tag{3}$$

It is represented by $a_f = \frac{k_f}{\rho c_p}$ in the equation. The density of the system air, whose temperature increases under the SCPP collector, decreases and begins to move upward. With the Boussinesq approach, the density of the system air depends on its temperature and the coefficient of thermal expansion (β) can be expressed as:

$$\beta = -\frac{1}{\rho}\left(\frac{\partial\rho}{\partial T}\right)_P \tag{3}$$

As can be seen from Equation (3), fluid density varies depending on temperature. In experimental data, the temperature change of the system air in the SCPP is low [14]. In this regard, the use of the Boussinesq approach is appropriate and the density of the system air can be presented with the following equation:

$$(\rho-\rho_o) \approx -\rho_o\beta(T-T_o) \tag{4}$$

It uses FLUENT equation (4) to estimate the density of the air in relation to the buoyancy force term in the momentum equation. One of the most important points to consider when evaluating SCPP performance is the characteristics of the system air. The flow characteristics of the system air must be interpreted before simulations are performed. The flow characteristic is important for the selection of the turbulence model in the FLUENT environment. Since heat transfer in SCPP occurs by natural convection, Rayleigh number (Ra) is taken as basis. Ra is given by the equation:

$$Ra = Gr\,Pr = \frac{g\beta\Delta TL^3}{a\nu} \tag{5}$$

β presented in the equation is the thermal expansion coefficient and is calculated with $\frac{1}{T_{max}}$. ΔT represents the amount of increase in the temperature of the system air under the collector, L represents the characteristic length, α represents the thermal dissipation and is equal to the ratio $\frac{k}{\rho c_p}$. Finally, ν is the kinematic viscosity. Gr and Pr represent Grashof and Prandtl numbers, respectively. Ra calculation details for the Manzanares pilot plant are given in Table 4.

After the value of 10^9 for the Ra number, the air flow in the system can be considered turbulent [49]. There are 3 different turbulence models in the FLUENT solver. There are researchers using these in the literature [8]. In this study, the RNG k-ε turbulence model, which gives better results in vortex and rotating flows, is preferred [52]. The equations and details of the model are as follows [49,57]:

$$\frac{\partial}{\partial x_i}(\rho k u_i) = \frac{\partial}{\partial x_j}\left[\alpha_k\mu_{eff}\frac{\partial k}{\partial x_j}\right] + G_k + G_b + \rho\varepsilon - Y_M + S_k \tag{6}$$

$$\frac{\partial}{\partial x_i}(\rho\varepsilon u_i) = \frac{\partial}{\partial x_j}\left[\alpha_\varepsilon\mu_{eff}\frac{\partial\varepsilon}{\partial x_j}\right] + C_{1_\varepsilon}\frac{\varepsilon}{k}(G_k + C_{3\varepsilon}G_b) - C_{2\varepsilon}\rho\frac{\varepsilon^2}{k} - R_e + S_\varepsilon \tag{7}$$

Turbulent kinetic energy production due to average velocity gradient in equation number 4,

$$G_k = -\rho u_i u_j\frac{\partial u_i}{\partial u_j} \tag{8}$$

Turbulent kinetic energy production due to buoyancy force,

$$G_b = \beta g_i\frac{\mu_t}{Pr_t}\frac{\partial_t}{\partial x_i} \tag{9}$$

The rate of dissipation due to fluctuating dilatation in compressible turbulence is

Table 4
Calculation of Rayleigh number for Manzanares SCPP [8].

Gravitational acceleration, g (m/s^2)	9.81
Thermal expansion coefficient, β (1/K)	0.003125
Temperature different, ΔT	20
Characteristic length, L (m)	1.85
Thermal diffusivity coefficient, a (m^2/s)	0.000021
Kinematic viscosity, ν (m^2/s)	0.0000148
Rayleigh Number, Ra	1.249×10^{10}

$$Y_M = 2\rho\varepsilon M_t^{\,2} \tag{10}$$

It is presented with. M_t in Equation (9) represents the Mach number for turbulent flow.

In addition, unlike the RNG k-ε standard turbulence model, the additional condition in this model is

$$R_\varepsilon = \frac{c_p\rho\eta^3\left(1-\frac{\eta}{\eta_o}\right)}{1+\beta\eta^3}\frac{\varepsilon^2}{k} \tag{11}$$

in equation η_o 4.38, β 0.012, and $\eta = \frac{S_k}{\varepsilon}$ [58].

SCPP absorbs direct and indirect solar radiation and transfers thermal energy to the system air. Modelling solar radiation is extremely important when performing system simulation. Discrete Ordinate (DO) radiation model is applied to the conducted study with the solar ray tracing algorithm. The heat transfer equation for the selected model is presented as follows [59]:

$$\nabla.\left[G\left(\underset{r}{\rightarrow},\underset{s}{\rightarrow}\right)\underset{s}{\rightarrow}\right] + (\alpha+\sigma_s)G\left(\underset{r}{\rightarrow},\underset{s}{\rightarrow}\right) = \alpha n^2\frac{\sigma T^4}{\pi} + \frac{\sigma_s}{4\pi}\int_0^{4\pi} G\left(\underset{r}{\rightarrow},\underset{s}{\rightarrow}'\right)\varpi\left(\underset{s}{\rightarrow}.\underset{s}{\rightarrow}'\right)d\Omega' \tag{12}$$

in the equation, $\overrightarrow{s}'$ is the scattering direction vector, α is the absorption coefficient, n is the refractive index, and σ_s is the scattering coefficient. Additionally, ϖ represents pase function, Ω' solid angle, and G represents solar radiation and has the unit W/m^2.

After the flow characteristics of the system, governing equations, and solar radiation modelling are presented, boundary conditions are introduced. It absorbs solar radiation with the SCPP collector. What makes this possible is that the collector is semi-permeable. In addition, it is assumed that the chimney is adiabatic and there is no pressure difference between the collector inlet and the chimney outlet. Additionally, heat transfer from the collector and the ground via convection is added to the model. Finally, in experimental data, it is seen that the temperature is constant at 305 K starting from 1 m below the ground [14]. For this reason, a temperature boundary condition is entered 1 m below the ground. Boundary conditions of the system are given in Table 5.

In the CFD model, glass is used as the collector material, steel construction is used as the chimney material based on the Manzanares pilot plant, and sand-gravel mixture is used as the ground. The physical properties of the materials used are given in Table 6. The collector in the system is semi-permeable and the chimney and floor are opaque. The system transfers 90 % of the solar radiation falling on the collector material. In addition, the thickness of the chimney material is 0.00125 m and the absorbency of the ground material is 0.9. RNG k-ε turbulence model is preferred as the turbulence model. Essentially, the error percentage resulting from the use of turbulence models is low. Fig. 4 shows the change of velocity values at the collector outlet and chimney entrance of the k-ε and k-ω turbulence models given in two equations, according to the chimney radius. When the graph is examined, it is understood that the effect of using different turbulence models is low. Therefore, the RNG k-ε turbulence model is adopted in this study because it is much more suitable for turbulent flows with high vorticity and its effects. As a solution method, the SIMPLE algorithm is executed for the relationship between air, velocity and pressure. Pressure interpolation is solved with the PRESTO technique. To model solar radiation, the solar ray tracing algorithm DO (discrete coordinates) is included in the simulation. For discretization, quadratic UPWIND is preferred. For the density of the system air, the Boussinesq approach is applied to the model. 10^{-6} is chosen for the convergence criterion. Climatic parameters and CFD details are given in Table 7.

There are different uses in the literature for power output calculation. In the study carried out, the calculations are made on the basis of the turbine pressure drop in the calculations made on the Manzanares pilot plant. For the pilot plant, the turbine pressure drop ratio is taken as 2/3. Power output (P_o) calculation is made by following the following equation [33]:

$$\mathrm{P_o} = \frac{2}{3}\mathrm{Q_v}\eta_{\mathrm{tur-gen}}\Delta\mathrm{P_{tur}} \tag{13}$$

Q_v presented in the equation represents the volumetric flow rate of the system and $n_{tur-gen}$ represents the turbine generator efficiency. ΔP_{tur} It represents the average pressure difference at the turbine location and is derived from CFD results at a height of 9 m inside the chimney, based on the turbine location of the pilot plant. The widely accepted value in the literature for turbine generator efficiency is 0.8, which is the same for the power output used in the initial data from the Manzanares pilot plant [8].

5. Mesh independence study and model validation

In this study, detailed analysis is made on the inclination angle of the SCPP collector and chimney. Based on the data, the optimum

Table 5
Boundary conditions for 3D CFD model [8].

Collector roof	Mixed (both radiation and convection), h = 10 W/m^2
Collector inlet	Pressure inlet, T_{amb} = 300 K and P_{gauge} = 0 Pa
Chimney outlet	Pressure outlet, P_{gauge} = 0 Pa
SCPP ground	Convection
Ground bottom	T = 305 K [14]
Chimney	Adiabatic (heat flux = 0)

Table 6
SCPP materials and properties [8,14].

Property/Material	Chimney	Collector	Ground
Density (kg/m^3)	2100	2500	2160
Specific heat cap. (J/kg.K)	880	750	710
Thermal conductivity (W/m.K)	1.4	1.15	1.84

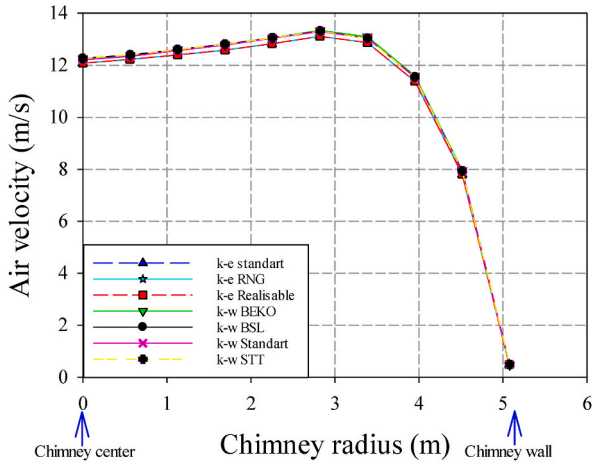

Fig. 4. Graph of velocity change depending on radius at the turbine location, according to turbulence models presented with two equations.

Table 7
CFD details and system air properties.

Solar radiation (W/(m^2)	1000
Ambient temperature (K)	300
Atmospheric pressure (Pa)	92,930
Air density (kg/m^3)	1.176 (Boussinesq)
Air conductivity (W/m.K)	0.0242
Kinematic viscosity (m^2/s)	1.52×10^{-5}
Stefan-Boltzmann constant (W/m^2.K^4)	5.67×10^{-8}
Thermal expansion coefficient (K^{-1})	0.0033

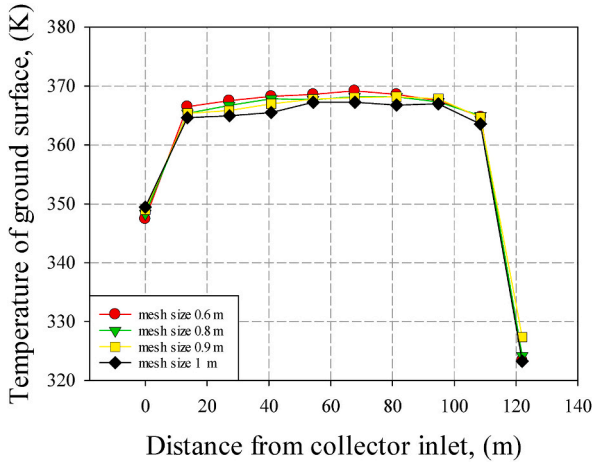

Fig. 5. Ground temperature chart according to collector inlet distance for different mesh sizes.

collector and chimney network of the Manzanares pilot plant is obtained. Then, the performance of the system is evaluated by changing the chimney height and collector size while maintaining the collector and chimney slope. First, it is tested that the results obtained from the 3D CFD model are independent of the number of cells. For this purpose, the temperature change on the ground is examined by changing the cell size within the range of 0.6–1 m. The detailed graph is given in Fig. 5. When the graph is examined, it is noticed that although the temperature change is remarkable up to a mesh size of 0.8 m, there is not much change for smaller mesh sizes. In this regard, a mesh size of 0.8 m is deemed sufficient for the model. Numerical data regarding mesh independent solution details are presented in Table 8. For the CFD model, it is understood that the temperature difference on the ground is evident until the mesh size is set to 0.8 m, but if the mesh size is further reduced, this difference is negligible. Additionally, when the performance outputs of the system are compared for different cell numbers, it is seen that the change after 0.8 m is negligible. Since it would not be economical to reduce the mesh size further, it is healthier to choose this mesh size.

After the mesh independent solution is obtained, the model is verified through experimental data and literature. In order to obtain reliable CFD results, the model used in the study is verified by using not only experimental data but also studies in the literature. The validation process relies on modelling with certain limitations. As illustrated in Table 9, environmental temperatures are set at 300 K and 293 K, while the solar radiation intensity is fixed at 1000 W/m^2. Nevertheless, for verification, experimental data is first consulted. In experimental data obtained from the pilot plant Manzanares, it is reported that the maximum air flow rate in the system is 15 m/s in no-load condition. Moreover, in experimental data, the maximum temperature on the ground is reported to exceed 70 °C. It is also stated in the same report that 48 kW power output was obtained from the system in the middle of the day. Table 9 presents the comparison of CFD results and experimental results. After the experimental data, the CFD model is compared with studies in the literature. Accordingly, temperature data on the ground are compared with the values in the researchers' studies. The relevant comparison is given in Fig. 6.

When the temperature distribution on the ground in CFD studies of different researchers is compared with the current study, differences are seen. For the conducted study, results are given for 293 and 300 K environmental temperatures and 1000 W/m^2 solar radiation intensity. Ming et al. [60] for an environmental temperature of 293.15 K at a solar radiation intensity of 800 W/m^2, Gholamalizadeh and Kim [61] 800 W/m^2, Pasumarthi and Sherif [62]. They present their results for midday climatic conditions of a typical summer day. From the graph, it can be seen that the researchers reached similar results with the study conducted, but there are some differences. It is understood that some researchers, in particular, obtained very high values for temperature and deviated from the experimental data. It is also known from experimental data that the temperature of the system air under the collector increases by 20 K. In this regard, lower temperatures are expected, especially towards the chimney entrance. The fact that the values obtained at both temperatures at the chimney entrance in the study was close to 320 K shows that the CFD results are sufficiently compatible with the experimental data.

6. Results and discussion

In this study, where the effects of collector slope and chimney slope on the system performance in SCPP are evaluated in detail, the optimum angle value is investigated. Since the studies in the literature are carried out under different conditions and with different definitions, there is space for studies detailing the collector slope and chimney slope for the Manzanares pilot plant. For this reason, the effect of the collector slope on the system is evaluated based on the pilot plant measurements. This effect is repeated for both higher and lower values of the collector inlet height, keeping the collector exit height constant at 1.85 m. When the collector inlet height is more than 1.85 m, the collector slope is evaluated as negative "-", and when the collector inlet height is less than 1.85 m, the collector slope is evaluated as positive "+". The power output plot of the system for a wide enough range of different values of the collector slope is given in Fig. 7. Note that for negative collector slope, the power output first increases slightly and then decreases. Therefore, the chart is terminated at this value. In addition, making the collector inlet height lower than 0.6° will reduce the performance of the system by causing reverse flows since the air entry into the system is blocked. Therefore, the graph is terminated at 0.6°, where the maximum power output is obtained. Collector slope is very important for the system. The agility of the collector, where solar energy is received directly into the system, supports upward movements within the system. It can be interpreted as normal that it gives more power output, especially since the positive slope collector provides this. The power output, which is 46.472 kW in the reference case, increases by 15.46 % and reaches 53.685 kW when the collector slope is 0.6. In particular, without changing the collector radius, the collector area becomes 52,368 m^2 in the reference case and 52,372 m^2 when the collector slope is 0.6°. The 4 m^2 collector area increase is negligible. In this regard, the performance increase achieved can provide serious cost reduction. For the given graph, the following equation can be used with 99.3 % accuracy by using the 5-parameter modified gaussian equation for the power output of the collector slope at different values:

Table 8
Mesh independent study for 3D CFD model.

Mesh size (m)	Elements number	Power output (kW)	% change Power output	Mass flow rate (kg/s)	% change mass flow rate
1	293,991	50.672	–	1104.848	–
0.9	399,302	45.816	−9.58	1074.392	−2.75
0.8	539,650	46.472	1.43	1079.696	0.49
0.6	947,888	45.951	−1.12	1080.856	0.107

Table 9
CFD model results comparison with experimental results.

Results	Max. air velocity (m/s)	Temperature rise in collector (K)	Power output (kW)
Experimental [14]	15	20	48
CFD results for 300 K	14.003	18.238	46.472
% difference	6.66	8.81	3.18
CFD results for 293 K	14.219	18.958	48.812
% difference	5.206	5.21	−1.69

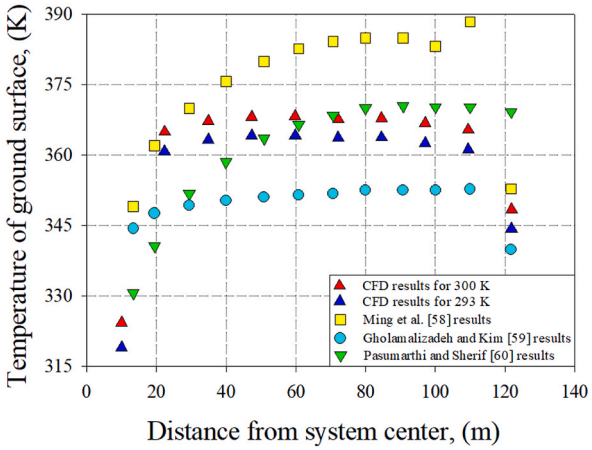

Fig. 6. Comparison of CFD results with studies in the literature on ground temperature.

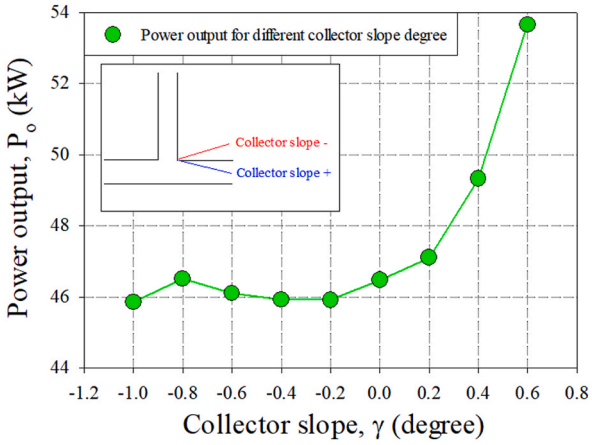

Fig. 7. Power output for different collector slope degree.

$$P_o = 70.3041 - 24.2358\, e^{\left[-0.5\left(\frac{|\gamma+0.7494|}{1.4152}\right)^{5.991}\right]} \quad (14)$$

There is general acceptance in the literature for the effect of chimney slope on SCPP performance. Researchers agree that divergent chimney design will have a positive impact on system performance. While evaluating the chimney angle values in the study, first the convergent and divergent chimney performance is compared. For this purpose, results are obtained by keeping the chimney entrance

Table 10
Comparison table of divergent and convergent chimney results.

Chimney angle	Max. air velocity (m/s)	Power output (kW)	Mass flow rate (kg/s)
−0.25° (Convergent chimney)	15.215	23.802	872.356
0.25° (Divergent chimney)	15.95	75.437	1268

area constant and changing the chimney exit area. Table 10 presents these results.

Decreasing the cross-sectional area at the chimney outlet means less air is discharged from the system. So much so that the mass flow rate, which is approximately 1080 kg/s in the reference case, decreases by approximately 20 % at −0.25° in the convergent chimney design. This situation is directly reflected in the power output. Although increasing the maximum air speed may cause error, it represents the maximum speed in the system. There is an increase in the maximum air flow rate due to the narrowing of the chimney exit area. Similarly, power output is low in the convergent chimney design. When all performance data are examined, it is clear that the divergent chimney design gives better performance, as is widely accepted in the literature. After this comparison, the performance of the system is examined against increasing values of the chimney divergence angle. Fig. 8 presents a graph of power output versus increasing chimney divergence angle. As can be seen from the graph, when the chimney inlet radius for the Manzanares pilot plant is kept constant at 5.08 m and the chimney divergence angle is increased, the maximum power output is obtained at 1.5°. After this point, the increase in the chimney divergence angle reduces the power output of the system. Compared to the reference case, with a flue divergence angle of 1.5°, the power output increases by 2.76 times, reaching 174.696 kW. The power output of the system for different chimney divergence angles in the given range can be calculated with the 4-parameter Log normal equation and the following equation:

$$P_o = 46.7755 + \frac{318.6185}{\lambda} e^{\left[-0.5\left(\frac{\ln\frac{\lambda}{3.9876}}{0.9382}\right)^2\right]} \quad (15)$$

After obtaining maximum performance values for collector slope and chimney slope, a model combining both situations are created, and its performance is examined. Comparison of the SCPP model with 1.5° chimney divergence angle and 0.6° collector slope with models containing only collector slope and only chimney slope is presented in Table 11.

When the results are compared, it is seen that the power output for the model including both slopes increased by 3.6 times compared to the reference case, reaching 216.853 kW. It is clear that the performance of the system increases further with the combined effect of both the chimney slope and the collector slope. Based on the maximum slope data obtained for the chimney and collector, the effect of changing the chimney height and collector size on the system is also evaluated while preserving these slope values. So much so that the chimney height is increased to 2.4 times for the Manzanares pilot plant while maintaining the chimney divergence angle at 1.5°. The power output graph for dimensionless chimney heights is given in Fig. 9.

When the graph is examined, it is seen that increasing the height of the chimney first increases the power output of the system exponentially, and then this increase decreases. In particular, it is seen that increasing the chimney height to 1.2 times the reference height is limiting for the exponential increase. According to the reference case, it is seen that using a chimney at this height will increase the power output by 1.4 times (303.269 kW). It can also be inferred from the graph that the chimney height will not lead to a continuous increase and is trending towards a convergence trend. For the data graph, the power output at different dimensionless chimney heights can be calculated with the following equation:

$$P_o = -13.81 + 75.5818\,H^* + 200.4163\,H^{*2} - 45.4197\,H^{*3} \quad (16)$$

The chimney is the driving force of the system and has a direct effect on increasing power output. A similar situation applies to the collector. Increasing the collector size will allow more solar energy to be included in the system, thus increasing the power output. The Manzanares pilot plant has a collector radius of 122 m. In this section, the collector size is changed by 0.2–1.2 times based on the pilot plant and its effect on power output is interpreted. Additionally, solutions for different chimney heights are repeated and changes in power output are compared. The power output graph according to the dimensionless collector radius for 3 different chimney heights is given in Fig. 10. It is seen that changing the collector radius has a more significant effect on the power output as the chimney height

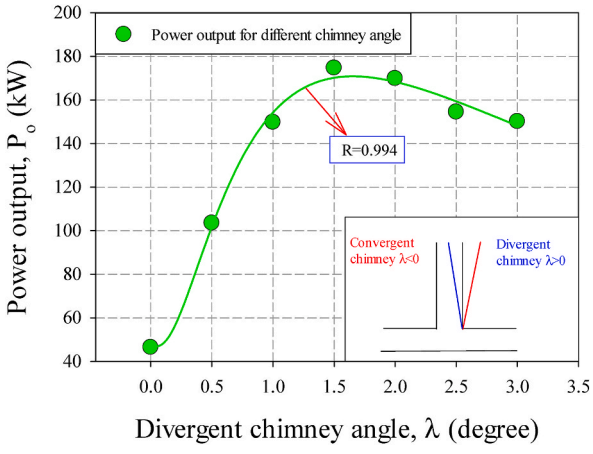

Fig. 8. Power output for different divergent chimney angle.

Table 11
Comparison of the results including only the collector slope and only the chimney slope with the model results including both slopes.

Model	Max. air velocity (m/s)	Power output (kW)	Mass flow rate (kg/s)
References model	14.003	46.472	1079.696
0.6° only collector slope	14.6	56.359	1145.752
1.5° only chimney slope	20.942	174.696	1688.3
Both collector and chimney slope	22.142	216.853	1818.188

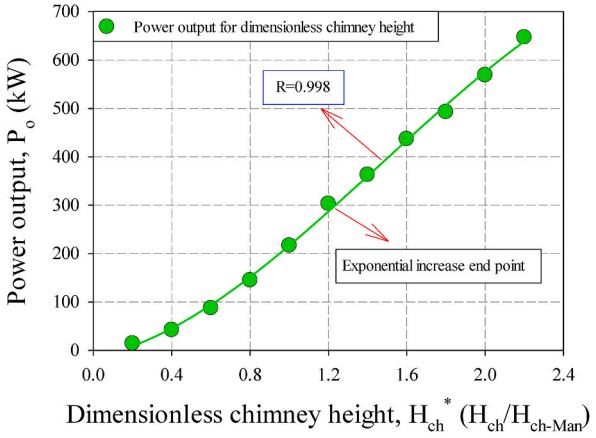

Fig. 9. Power output for different dimensionless chimney heights.

increases. When the chimney height is kept at the reference size, increasing the collector size by 1.2 times increases the power output by 52.46 %, reaching 330 kW. When the chimney height is reduced to 80 % of the reference size, increasing the collector radius by 1.2 times from the reference case increases the power output by 59.5 %–231.584 kW. When the chimney height is reduced to 60 % compared to the reference state, increasing the collector radius to 1.2 times the reference state increases the power output by 48.84 %–130.26 kW. It is understood from these results that increasing the collector radius increases the power output more at larger chimney heights. Power output values according to the dimensionless collector radius for 3 different chimney heights respectively can be found with the following equations:

$$\text{For } H_{ch} = 194.6^{*}1 \; P_o = 4.202 - 3.5229\, R_{coll}{}^{*} + 165.05\, R_{coll}{}^{*2} + 53.4479\, R_{coll}{}^{*3} \tag{17}$$

$$\text{For } H_{ch} = 194.6^{*}0.8 \; P_o = -8.584 + 75.5722\, R_{coll}{}^{*} - 36.2521\, R_{coll}{}^{*2} + 118.559\, R_{coll}{}^{*3} \tag{18}$$

$$\text{For } H_{ch} = 194.6^{*}0.6 \; P_o = -1.1233 + 7.4244\, R_{coll}{}^{*} + 61.1239\, R_{coll}{}^{*2} + 19.9387\, R_{coll}{}^{*3} \tag{19}$$

The results confirm the results in the literature and are explanatory, especially for collector slope and chimney slope. In addition, in order to better interpret the effect of the change in collector radius, it is necessary to make separate analysis for each case by evaluating

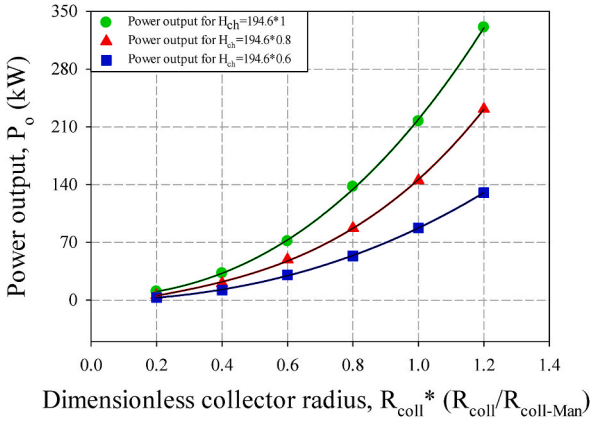

Fig. 10. Power output graph for dimensionless collector radius at different chimney heights.

the system at different chimney heights. In future studies, we will focus on sizing the ideal power output by making cost analysis.

7. Exploring output estimation with neural networks

Artificial neural networks, or ANNs, are undergoing a paradigm change as they emerge from the limitations of conventional approaches. In contrast to traditional methods, ANNs benefit from large amounts of input/output data and do not require particular structural requirements. These networks show remarkable ability to identify both linear and nonlinear correlations in input-output data after careful training [63–69]. Their ability to adjust to new knowledge is a result of ongoing retraining. Utilizing input-output data is the first step in creating an effective ANN algorithm. This flexibility, enabled by ANNs, opens up new possibilities for comprehending intricate data patterns and improves problem-solving abilities. Because of their adaptability, ANNs are significant resources in a variety of fields. Notably, they have gained prominence in recent times, particularly within various initiatives in solar energy systems. Ongoing research underscores the significance of ANNs in predicting system performance [70,71]. In the present study, employing ANN to estimate the power output data of SCPP—an innovative and invaluable power generation system leveraging solar energy—is planned.

In present study, as shown in Fig. 11, neural network designs typically consist of three layers: the input layer, the output layer, and one or more hidden layers. The system's inputs are represented by five neurons in the input layer, which stand for the collector intake (h_i), collector radius (R_c), collector slope (γ), chimney height (h_c), and divergence angle (λ). In the meantime, one neuron representing power (PO [kW]) is present in the output layer.

The training dataset, validation dataset, and testing dataset are the three main parts of dataset segmentation. By modifying the network in response to mistakes made, the training dataset makes neural network training easier. Next, the validation dataset evaluates the generalization of the network and determines when to stop training if generalization is not improving. Lastly, network performance is assessed both during and after training using the testing dataset. This specific architecture sets aside 85 % of the entire dataset for training, 10 % for testing, and the remaining percentage for evaluating network performance. The complexity and flexibility of this design highlight the increasing significance of ANNs in transforming methods for problem-solving and data analysis.

To determine the ideal number of hidden layer neurons in our Artificial Neural Network (ANN), we used Root Mean Square Error (RMSE) as a key parameter. Computed as

$$\mathrm{RMSE} = \sqrt{\frac{1}{n}\sum_{k=1}^{n}\left(y_{pr} - y_{ta}\right)^2} \tag{20}$$

where 'n' denotes the total size of the dataset, 'y_{ta}' represents the actual (target) output, and 'y_{pr}' represents the expected output produced by the trained ANN. We measured the network's prediction accuracy (RMSE) to determine the most successful design. This strategy allowed us to fine-tune the ANN's design, improving its capacity to detect complicated patterns and correlations in the data. Ultimately, our goal was to enhance the network's performance in accurately predicting outputs, contributing to its effectiveness in various applications. A lower RMSE shows that the ANN can better predict the actual results. In this case, the procedure is directed by a precisely created flowchart, as shown in Fig. 12. This flowchart provides a methodical framework for determining the optimal configuration for hidden neurons, which have a substantial impact on the network's performance.

Now we systematically varied the number of hidden layer neurons and displayed the resulting RMSE trends, as shown in Fig. 13. The horizontal axis is denoted as "No. of neurons," while the vertical axis is labeled "RMSE," representing Root Mean Square Error. RMSE serves as a standard measure to evaluate the alignment between a machine learning model's predictions and the actual outcomes. Within the plot, RMSE values range from 0.4 to 0.1 on the y-axis, while the x-axis spans from 2 to 20 neurons. Notably, there is an observable trend where RMSE tends to decrease/increase as the number of neurons rises. This pattern suggests that lower RMSE values are associated with a higher number of neurons in the model, indicating improved prediction accuracy with increased neural network complexity. Fig. 13 illustrates that using 9 neurons in the hidden layer results in the ideal RMSE of 0.0054. This approach is consistent with the goal of reducing the average squared gap between predicted and target values, highlighting the neural network model's accuracy.

Moving on to Fig. 14, we observe the fluctuations in Mean Squared Error (MSE) across different epochs for the training, validation, and testing datasets. Notably, at epoch 141, the MSE stands at 0.0010251, indicating optimal validation performance. However, proceeding beyond this point leads to an escalation in errors attributed to repetitive iterations. Consequently, a decision is made to halt further training to mitigate error propagation. The meticulous assessment of MSE trends throughout epochs ensures the identification of the epoch where the neural network achieves its best performance on the validation set, serving as a crucial determinant for concluding the training process. This careful approach ensures that the neural network is trained effectively, balancing between achieving high performance and preventing over fitting.

Thus, our artificial neural network's hidden layer has 9 neurons. The linear regression value is calculated based on the correlation between results and goals. A score of 1 suggests a high association, whereas 0 implies otherwise. Fig. 15 shows regression for several datasets. The illustrations show that the regression factor approaches one, demonstrating a strong relationship between the input and modelled datasets inside this neural network.

Using the trained network, we calculated predicted output values for many datasets. Fig. 15 depicts the distribution of goal and projected values at the output (PO) across many datasets.

In this bar plot (Fig. 16), each bar corresponds to the output of original and predicted values for specific parameter sets:

The corresponding values from a1 to a13 are described in Table 12. Fig. 15 shows that our neural network of nine neurons

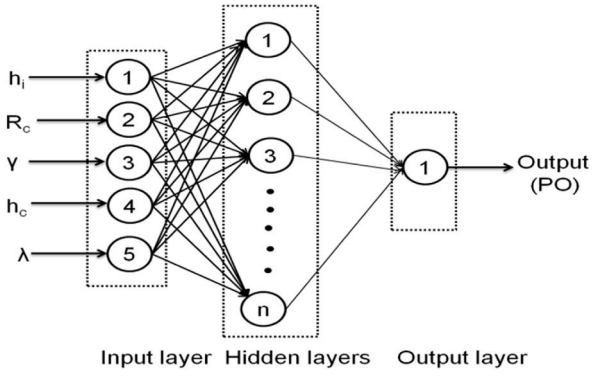

Fig. 11. The organized structure of a three-layer neural network.

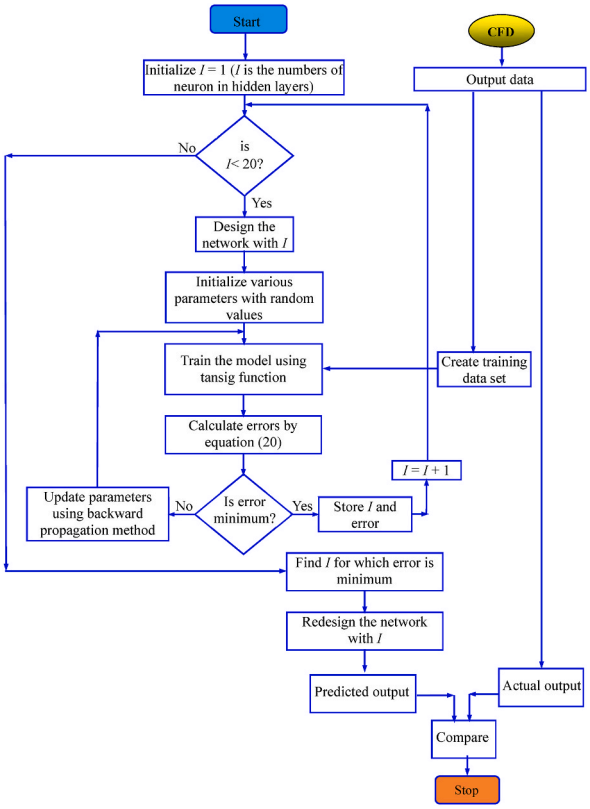

Fig. 12. A Flowchart guiding CFD and the determination of neuron count in the hidden layer.

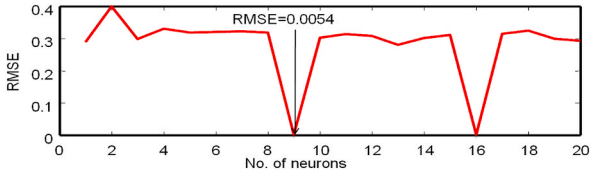

Fig. 13. The variation between the RMSE and the number of neurons in the hidden layer.

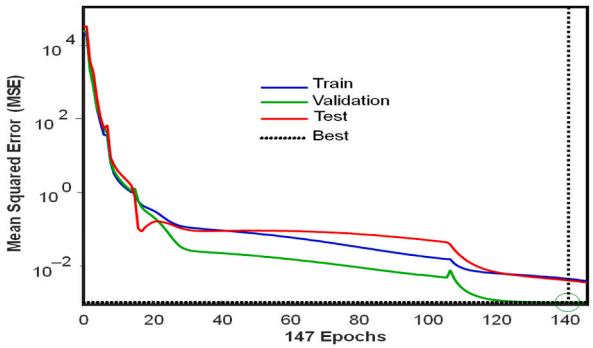

Fig. 14. Depicts the variations in MSE across epochs for the various data sets.

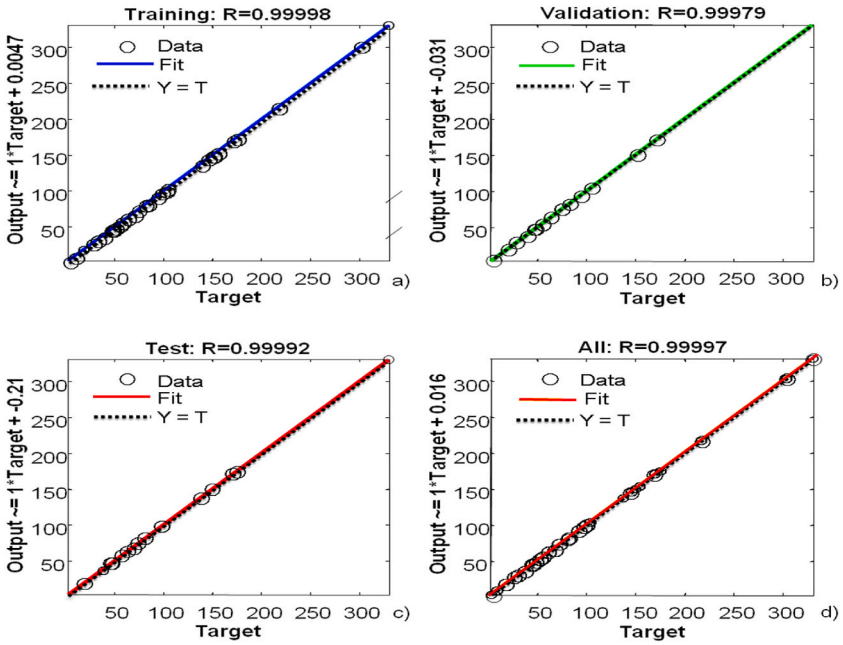

Fig. 15. Depicts the linear regression fitted to the input data alongside the modelled data which is shown as four types of datasets: a) training, b) validation, c) testing, and d) overall.

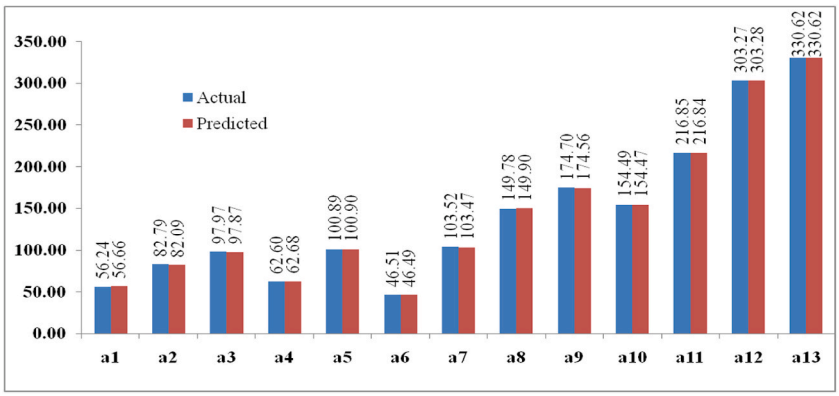

Fig. 16. Showcases a bar plot illustrating the different values of the dataset for both actual output and predicted output.

Table 12
Details of different sets of SCPP.

set	h_i	R_c	γ	h_c	λ
a1	1.85	122	0	116.76	0
a2	1.85	122	0	350.28	0
a3	1.85	122	0	428.12	0
a4	1.85	146	0	194.6	0
a5	1.85	195	0	194.6	0
a6	3.55	122	0	194.6	0
a7	1.85	122	0.8	194.6	0.5
a8	1.85	122	0	194.6	1
a9	1.85	122	0	194.6	1.5
a10	1.85	122	0	194.6	2.5
a11	0.57	122	0.6	233.52	1.5
a12	0.57	122	0.6	233.52	1.5
a13	0.313	146.4	0.6	194.6	1.5

appropriately predicts the output values. As a result, we can predict output values for an unknown dataset using this trained neural network.

8. Conclusion

SCPP is one of the large-scale systems that can provide power output with the solar energy it absorbs thanks to its collector and the continuous pressure difference provided by its high chimney. In this study, optimum values for collector slope and chimney slope are presented based on the Manzanares SCPP pilot plant measurements. Additionally, the effect of the change in chimney height and collector radius on the system power output is included. The study is carried out with a 3D CFD model and new results are obtained in the light of experimental data and validation from the literature. However, the inquiry does not finish its mission with these validations and results. Following these assessments, the study introduces a novel perspective by employing the ANN method to gauge SCPP system performance. Critical findings from the study are as follows:

- For SCPP modelling, the 3D CFD model gives consistent results. So much so that CFD results are quite compatible with experimental data and literature.
- At 1000 W/m^2 solar radiation intensity and 300 K environmental temperature, 46.472 kW power output is obtained from CFD. This value is 48 kW in experimental data.
- Starting temperature has a significant impact on power output. In fact, the power output of the system, which gives a power output of 46.472 kW at 300 K, increases by 5 %–48,812 kW at 293 K ambient temperature.
- For the Manzanares pilot plant, the divergent stack design yields greater power output than the convergent stack design.
- The optimum value of the divergent chimney angle in the reference measurements for the Manzanares pilot plant is 1.5°. At this angle value, the power output of the system is 174.696 kW. Increasing this angle value decreases the power output.
- The slope value that gives the maximum power output for the collector is 0.6°. When the collector outlet height is kept constant and the collector inlet height is reduced to 0.57 m, the system gives maximum power output (53.658 kW). This power output is 15.46 % higher than the power output of the horizontal collector in the reference case.
- If the chimney divergence angle of the Manzanares pilot plant is made 1.5° and the collector slope is 0.6° without changing the chimney height and collector radius, the system gives 216.853 kW power output at 1000 W/m^2 solar radiation intensity and 300 K environmental temperature. This value is 3.66 times higher than the reference case of 46.472 kW.
- Increasing the chimney height of a system with a sloped collector and chimney increases the power output exponentially up to a point. Increasing the chimney height by 20 % compared to the reference case increases the power output by 39.85 %–303.269 kW. After this point, increasing the chimney height increases the power output, but a convergence trend appears to begin.
- Increasing the collector size at different chimney heights has different effects on the system. As the chimney height increases, the effect of the change in collector size on the power output is more evident.
- The validation process confirms the accuracy of the predictions generated using the ANN method, with the chosen 9 neurons in the hidden layer demonstrating impeccable alignment with the study data.

CRediT authorship contribution statement

Pinar Mert Cuce: Writing – review & editing, Writing – original draft, Methodology, Formal analysis, Conceptualization. **Erdem Cuce:** Writing – review & editing, Supervision, Methodology, Investigation. **Dipak Kumar Mandal:** Writing – review & editing, Formal analysis. **Dilip Kumar Gayen:** Writing – review & editing. **Muhammad Asif:** Writing – review & editing, Formal analysis. **Abdallah Bouabidi:** Writing – review & editing. **Saad Alshahrani:** Writing – review & editing, Funding acquisition. **Chander Prakash:** Writing – review & editing. **Manzoore Elahi M. Soudagar:** Writing – review & editing.

Declaration of competing interest

The authors declare that they have no known competing financial interests or personal relationships that could have appeared to

influence the work reported in this paper.

Data availability

No data was used for the research described in the article.

Acknowledgements

The authors extend their appreciation to the Deanship of Research and Graduate Studies at King Khalid University for funding this work through Large Research Project under grant number RGP2/171/45.

Nomenclature

α	Thermal dissipation
ν	Kinematic viscosity (m^2/s)
λ	Divergent chimney angle (°)
γ	Collector angle (°)
β	Thermal expansion coefficient (1/K)
ρ	Density (kg/m^3)
ρ_o	Ambient density (kg/m^3)
g	Gravitational acceleration (m/s^2)
η	Efficiency
ΔT	Temperature difference (K)
L	Characteristic length (m)
k	Thermal conductivity (W/mK)
c_p	Heat capacity (J/gK)
R	Radius (m)
D	Diameter (m)
T	Temperature (K)
P	Pressure (Pa)
P_o	Power output (kW)
Gr	Grashof number
Ra	Rayleigh number
Ch	Chimney
Coll	Collector
CFD	Computational fluid dynamics
AR	Area ratio
SCPP	Solar chimney power plant
SUT	Solar updraft tower
Man	Manzanares
H*	Dimensionless height
R*	Dimensionless radius

References

[1] A.T. Doppalapudi, A.K. Azad, M.M.K. Khan, Advanced strategies to reduce harmful nitrogen-oxide emissions from biodiesel fueled engine, Renew. Sustain. Energy Rev. 174 (Mar. 2023) 113123, https://doi.org/10.1016/j.rser.2022.113123.

[2] M.P. Pablo-Romero, A. Sánchez-Braza, A. Galyan, Renewable energy use for electricity generation in transition economies: evolution, targets and promotion policies, Renew. Sustain. Energy Rev. 138 (Mar. 2021) 110481, https://doi.org/10.1016/j.rser.2020.110481.

[3] K. Verhaegen, L. Meeus, B. Delvaux, R. Belmans, Electricity produced from renewable energy sources-What target are we aiming for? Energy Pol. 35 (11) (2007) https://doi.org/10.1016/j.enpol.2007.06.004.

[4] A. Qazi, et al., Towards sustainable energy: a systematic review of renewable energy sources, technologies, and public opinions, IEEE Access 7 (2019) 63837–63851, https://doi.org/10.1109/ACCESS.2019.2906402.

[5] P.A. Owusu, S. Asumadu-Sarkodie, A review of renewable energy sources, sustainability issues and climate change mitigation, Cogent Eng. 3 (1) (Dec. 2016) 1167990, https://doi.org/10.1080/23311916.2016.1167990.

[6] G.E. Halkos, E.-C. Gkampoura, Reviewing usage, potentials, and limitations of renewable energy sources, Energies 13 (11) (Jun. 2020) 2906, https://doi.org/10.3390/en13112906.

[7] E. Cuce, P.M. Cuce, H. Sen, Numerical Analysis of the Effect of Collector Height in Solar Chimney Power Plants, in: ISPEC 15th International Conference on Engineering and Natural Sciences, 04-06 March 2023. Muş, Turkey.

[8] E. Cuce, et al., Solar chimney power plants: a review of the concepts, designs and performances, Sustainability 14 (3) (Jan. 2022) 1450, https://doi.org/10.3390/su14031450.

[9] H. Sen, E. Cuce, Dynamic Pressure Distributions in Solar Chimney Power Plants: A Numerical Research for the Pilot Plant in Manzanares, Spain, WSSET Newsletter, 2020, 12 (1), 2–2.

[10] X. Zhou, Y. Xu, Solar updraft tower power generation, Sol. Energy 128 (Apr. 2016) 95–125, https://doi.org/10.1016/j.solener.2014.06.029.
[11] A. Dhahri and A. Omri, "A Review of Solar Chimney Power Generation Technology".
[12] J. Schlaich, R. Bergermann, W. Schiel, G. Weinrebe, Design of commercial solar updraft tower systems—utilization of solar induced convective flows for power generation, J. Sol. Energy Eng. 127 (1) (Feb. 2005) 117–124, https://doi.org/10.1115/1.1823493.
[13] T. Ming (Ed.), Solar Chimney Power Plant Generating Technology, Academic Press, 2016.
[14] W. Haaf, Solar chimneys, Int. J. Sol. Energy 2 (2) (Jan. 1984) 141–161, https://doi.org/10.1080/01425918408909921.
[15] W. Haaf, K. Friedrich, G. Mayr, J. Schlaich, Solar chimneys Part I: principle and construction of the pilot plant in Manzanares, Int. J. Sol. Energy 2 (1) (Jan. 1983) 3–20, https://doi.org/10.1080/01425918308909911.
[16] L.B. Mullett, The solar chimney—overall efficiency, design and performance, Int. J. Ambient Energy 8 (1) (Jan. 1987) 35–40, https://doi.org/10.1080/01430750.1987.9675512.
[17] J. Schlaich, The Solar Chimney: Electricity from the Sun, 1995.
[18] E. Cuce, H. Sen, Solar chimney power plants from past to present: performance parameters affecting system power output, Euro Asia 7th Int. Congr. Appl. Sci. 21–22 (2020) 256–262.
[19] E. Cuce, et al., Performance assessment of solar chimney power plants with natural thermal energy storage materials on ground: CFD analysis with experimental validation, Int. J. Low Carbon Technol. 17 (Feb. 2022) 752–759, https://doi.org/10.1093/ijlct/ctac001.
[20] S.M. Raney, J.R. Brooks, J.P. Schaffer, J.J. French, Experimental validation of solar chimney performance models and operational characteristics for small scale remote applications, in: ASME 2012 6th International Conference on Energy Sustainability, Parts A and B, American Society of Mechanical Engineers, Jul. 2012, pp. 27–32, https://doi.org/10.1115/ES2012-91192.
[21] T. Mekhail, A. Rekaby, M. Fathy, M. Bassily, R. Harte, Experimental and theoretical performance of mini solar chimney power plant, J. Clean Energy Technol. 5 (4) (Jul. 2017) 294–298, https://doi.org/10.18178/JOCET.2017.5.4.386.
[22] E. Cuce, P.M. Cuce, H. Sen, A thorough performance assessment of solar chimney power plants: case study for Manzanares, Clean Eng. Technol. 1 (Dec. 2020) 100026, https://doi.org/10.1016/j.clet.2020.100026.
[23] P. Guo, J. Li, Y. Wang, Numerical simulations of solar chimney power plant with radiation model, Renew. Energy 62 (Feb. 2014) 24–30, https://doi.org/10.1016/j.renene.2013.06.039.
[24] A.B. Kasaeian, M. Amirifard, M.H. Ahmadi, F. Kasaeian, Investigation of the effects of ambient temperature and dimensional parameters on the performance of solar chimney power plants, Int. J. Low Carbon Technol. (Mar. 2017) 1–14, https://doi.org/10.1093/ijlct/ctw016.
[25] P. Guo, J. Li, Y. Wang, Annual performance analysis of the solar chimney power plant in Sinkiang, China, Energy Convers. Manag. 87 (Nov. 2014) 392–399, https://doi.org/10.1016/j.enconman.2014.07.046.
[26] H. Hoseini, R. Mehdipour, Performance evaluation of hybrid solar chimneys for fresh water production, Environ. Prog. Sustain. Energy 39 (1) (Jan. 2020), https://doi.org/10.1002/ep.13276.
[27] J. Schlaich, R. Bergermann, W. Schiel, G. Weinrebe, Design of commercial solar updraft tower systems—utilization of solar induced convective flows for power generation, J. Sol. Energy Eng. 127 (1) (Feb. 2005) 117–124, https://doi.org/10.1115/1.1823493.
[28] E. Cuce, H. Sen, P.M. Cuce, Numerical performance modelling of solar chimney power plants: influence of chimney height for a pilot plant in Manzanares, Spain, Sustain. Energy Technol. Assessments 39 (2020), https://doi.org/10.1016/j.seta.2020.100704.
[29] A. Koonsrisuk, S. Lorente, A. Bejan, Constructal solar chimney configuration, Int. J. Heat Mass Tran. 53 (1–3) (Jan. 2010) 327–333, https://doi.org/10.1016/j.ijheatmasstransfer.2009.09.026.
[30] J. Li, P. Guo, Y. Wang, Effects of collector radius and chimney height on power output of a solar chimney power plant with turbines, Renew. Energy 47 (Nov. 2012) 21–28, https://doi.org/10.1016/j.renene.2012.03.018.
[31] X. Zhou, J. Yang, B. Xiao, G. Hou, F. Xing, Analysis of chimney height for solar chimney power plant, Appl. Therm. Eng. 29 (1) (2009), https://doi.org/10.1016/j.applthermaleng.2008.02.014.
[32] A.B. Kasaeian, Sh Molana, K. Rahmani, D. Wen, A review on solar chimney systems, Renew. Sustain. Energy Rev. 67 (Jan. 2017) 954–987, https://doi.org/10.1016/j.rser.2016.09.081.
[33] H. Şen, A.P. Mert Cüce, E. Cüce, Impacts of collector radius and height on performance parameters of solar chimney power plants: a case study for Manzanares, Spain, Recep Tayyip Erdoğan Üniversitesi Fen ve Mühendislik Bilimleri Dergisi 2 (2) (Dec. 2021) 83–104, https://doi.org/10.53501/rteufemud.1017909.
[34] P. Karimipour-Fard, H. Beheshti, Performance enhancement and environmental impact analysis of a solar chimney power plant: twenty-four-hour simulation in climate condition of Isfahan Province, Iran, Int. J. Eng. 30 (8) (2017) 1260–1269.
[35] E. Cuce, H. Sen, P. Mert Cuce, Collector factor in a solar chimney power plant: CFD analysis for the pilot plant in Manzanares, Energetika 68 (1) (Jan. 2023), https://doi.org/10.6001/energetika.v68i1.4856.
[36] S.R. Rajpu, S.R. Nigam, M. Sen, Integrated solar heat and wind power plant: design and performance, Int. J. Energy Sect. Manag. 7 (2017) 407–423.
[37] P. Mert Cuce, H. Şen, E. Cuce, Impact of tower diameter on power output in solar chimney power plants, Gazi J. Eng. Sci. 7 (3) (Dec. 2021) 253–263, https://doi.org/10.30855/gmbd.2021.03.08.
[38] A. Dhahri, A. Omri, J. Orfi, Study of the Influence of Geometric Parameters on a Solar Chimney Power Plants System, 2013.
[39] P.J. Cottam, P. Duffour, P. Lindstrand, P. Fromme, Effect of canopy profile on solar thermal chimney performance, Sol. Energy 129 (May 2016) 286–296, https://doi.org/10.1016/j.solener.2016.01.052.
[40] A.B. Kasaeian, E. Heidari, S.N. Vatan, Experimental investigation of climatic effects on the efficiency of a solar chimney pilot power plant, Renew. Sustain. Energy Rev. 15 (9) (Dec. 2011) 5202–5206, https://doi.org/10.1016/J.RSER.2011.04.019.
[41] M. Ghalamchi, A. Kasaeian, M. Ghalamchi, Experimental study of geometrical and climate effects on the performance of a small solar chimney, Renew. Sustain. Energy Rev. 43 (Mar. 2015) 425–431, https://doi.org/10.1016/J.RSER.2014.11.068.
[42] M. J. Ahirwar and P. Sharma, "Analyzing the effect of solar chimney power plant by varying chimney height, collector slope and chimney diverging angle," Int. J. Innov. Res. Technol., vol. 6, no. 7, pp. 213–219.
[43] E. Gholamalizadeh, M.-H. Kim, Multi-objective optimization of a solar chimney power plant with inclined collector roof using genetic algorithm, Energies 9 (11) (Nov. 2016) 971, https://doi.org/10.3390/en9110971.
[44] H. Nasraoui, Z. Driss, A. Ayedi, H. Kchaou, Numerical and experimental study of the aerothermal characteristics in solar chimney power plant with hyperbolic chimney shape, Arabian J. Sci. Eng. 44 (9) (Sep. 2019) 7491–7504, https://doi.org/10.1007/s13369-019-03821-x.
[45] A. Bouabidi, A. Ayadi, H. Nasraoui, Z. Driss, M.S. Abid, Study of solar chimney in Tunisia: effect of the chimney configurations on the local flow characteristics, Energy Build. 169 (Jun. 2018) 27–38, https://doi.org/10.1016/j.enbuild.2018.01.049.
[46] H. Nasraoui, Z. Driss, A. Ayadi, A. Bouabidi, H. Kchaou, Numerical and experimental study of the impact of conical chimney angle on the thermodynamic characteristics of a solar chimney power plant, Proc. IME E J. Process Mech. Eng. 233 (5) (Oct. 2019) 1185–1199, https://doi.org/10.1177/0954408919859160.
[47] P. Das, V.P. Chandramohan, 3D numerical study on estimating flow and performance parameters of solar updraft tower (SUT) plant: impact of divergent angle of chimney, ambient temperature, solar flux and turbine efficiency, J. Clean. Prod. 256 (May 2020) 120353, https://doi.org/10.1016/j.jclepro.2020.120353.
[48] E. Cuce, A. Saxena, P.M. Cuce, H. Sen, S. Guo, K. Sudhakar, Performance assessment of solar chimney power plants with the impacts of divergent and convergent chimney geometry, Int. J. Low Carbon Technol. 16 (3) (2021), https://doi.org/10.1093/ijlct/ctaa097.
[49] D. Kumar Mandal, N. Biswas, N.K. Manna, A.C. Benim, Impact of chimney divergence and sloped absorber on energy efficacy of a solar chimney power plant (SCPP), Ain Shams Eng. J. (Jul. 2023) 102390, https://doi.org/10.1016/j.asej.2023.102390.
[50] Y. Xu, X. Zhou, Performance of divergent-chimney solar power plants, Sol. Energy 170 (Aug. 2018) 379–387, https://doi.org/10.1016/j.solener.2018.05.068.
[51] S. Hu, D.Y.C. Leung, J.C.Y. Chan, Impact of the geometry of divergent chimneys on the power output of a solar chimney power plant, Energy 120 (2017), https://doi.org/10.1016/j.energy.2016.12.098.

[52] A. Hassan, M. Ali, A. Waqas, Numerical investigation on performance of solar chimney power plant by varying collector slope and chimney diverging angle, Energy 142 (Jan. 2018) 411–425, https://doi.org/10.1016/j.energy.2017.10.047.
[53] H.H. Al-Kayiem, Q.A. Al-Nakeeb, Geometry alteration effect on the performance of a solar-wind power system, in: Proceedings of the International Conference on Energy and Environment, University Tenaga National-Malaysia, Aug. 2006, pp. 50–55.
[54] B.K. Behera, K.K. Sharma, S.S. Sahoo, S. Kumar, Rating and sizing analysis of the solar chimney power plant considering uncertainty in solar radiation and under different load conditions, Energy Sources, Part A Recovery, Util. Environ. Eff. 45 (4) (2023) 12535–12552.
[55] B. K. Behera, K. K. Sharma, S. S. Sahoo, and S. Kumar, "Techno feasibility study and optimum sizing evaluation of an industrial-level solar chimney power plant with a storage system: a case study in Mumbai, India," Environ. Prog. Sustain. Energy, e14365.
[56] S.A. Abdul Hussein, M.A. Nima, Numerical and experimental investigation of semicircular solar updraft tower system employing porous copper metal foam, J. Eng. Sustain. Dev. 27 (5) (Sep. 2023) 596–614, https://doi.org/10.31272/jeasd.27.5.4.
[57] E. Cuce, H. Sen, P.M. Cuce, Numerical performance modelling of solar chimney power plants: influence of chimney height for a pilot plant in Manzanares, Spain, Sustain. Energy Technol. Assessments 39 (Jun. 2020) 100704, https://doi.org/10.1016/j.seta.2020.100704.
[58] M.A.H. Abdelmohimen, S.A. Algarni, Numerical investigation of solar chimney power plants performance for Saudi Arabia weather conditions, Sustain. Cities Soc. 38 (2018), https://doi.org/10.1016/j.scs.2017.12.013.
[59] Fluent Inc, ANSYS FLUENT, 2010.
[60] T. Ming, W. Liu, Y. Pan, G. Xu, Numerical analysis of flow and heat transfer characteristics in solar chimney power plants with energy storage layer, Energy Convers. Manag. 49 (10) (Oct. 2008) 2872–2879, https://doi.org/10.1016/j.enconman.2008.03.004.
[61] E. Gholamalizadeh, M.-H. Kim, Three-dimensional CFD analysis for simulating the greenhouse effect in solar chimney power plants using a two-band radiation model, Renew. Energy 63 (Mar. 2014) 498–506, https://doi.org/10.1016/j.renene.2013.10.011.
[62] N. Pasumarthi, S.A. Sherif, Experimental and theoretical performance of a demonstration solar chimney model—Part I: mathematical model development, Int. J. Energy Res. 22 (3) (Mar. 1998) 277–288, https://doi.org/10.1002/(SICI)1099-114X(19980310)22:3<277::AID-ER380>3.0.CO;2-R.
[63] S. Amirkhani, Sh Nasirivatan, A.B. Kasaeian, A. Hajinezhad, ANN and ANFIS models to predict the performance of solar chimney power plants, Renew. Energy 83 (2015) 597–607.
[64] N. Fadaei, W.-M. Yan, M.M. Tafarroj, A. Kasaeian, The application of artificial neural networks to predict the performance of solar chimney filled with phase change materials, Energy Convers. Manag. 171 (2018) 1255–1262.
[65] P.G. Asteris, V.G. Mokos, Concrete compressive strength using artificial neural networks, Neural Comput. Appl. 32 (2020) 11807–11826.
[66] S. Rostami, D. Toghraie, B. Shabani, B, et al., Measurement of the thermal conductivity of MWCNT-CuO/water hybrid nanofluid using artificial neural networks (ANNs), J. Therm. Anal. Calorim. 143 (2021) 1097–1105.
[67] P. Faghihi, A. Jalali, An artificial neural network-based optimization of reverse electrodialysis power generating cells using CFD and genetic algorithm, Int. J. Energy Res. 46 (2022) 21217–21233.
[68] N. Matera, D. Mazzeo, C. Baglivo, P.M. Congedo, Hourly forecasting of the photovoltaic electricity at any latitude using a network of artificial neural networks, Sustain. Energy Technol. Assessments 57 (2023) 103197.
[69] D.K. Mandal, N. Biswas, N.K. Manna, D.K. Gayen, An application of Artificial Neural Network (ANN) for comparative performance assessment of solar chimney (SC) plant for green energy production, Sci. Rep. 14 (2024) 979.
[70] E. Ghandourah, Y.S. Prasanna, A.H. Elsheikh, E.B. Moustafa, M. Fujii, S.S. Deshmukh, Performance prediction of aluminum and polycarbonate solar stills with air cavity using an optimized neural network model by golden jackal optimizer, Case Stud. Therm. Eng. 47 (2023) 103055.
[71] J. Ruelas, F. Munoz, J. Palomares, J. Delfin, B. Lucero, Energy performance of a solar cavity receiver with neural output flow regulation under controlled conditions, Case Stud. Therm. Eng. 36 (2022) 102219.